

619. Application of extended time-frequency domain average in ultrasonic detecting

Yanxue Wang^{a,b}, Zhengjia He^b, Jiawei Xiang^a

^aSchool of Mechanical and Electrical Engineering, Guilin University of Electronic Technology, Guilin, 541004, China.

^bSchool of Mechanical Engineering, Xi'an Jiaotong University, 710049, Xi'an, China

E-mail: *Yan.Xue.Wang@gmail.com (Y. X. Wang)*

(Received 10 February 2011; accepted 15 May 2011)

Abstract. Ultrasonic signal detection is essential for the ultrasonic-based applications such as ultrasonic flow measurements and nondestructive testing. The paper proposes three extended time-frequency domain average (ETFDA) techniques, which are based on the smoothed pseudo-Wigner-Ville distribution, continuous wavelet transform and Hilbert-Huang transform. These techniques combine beneficial time-frequency localization characteristics of the time-frequency analysis and abilities of the time domain averaging (TDA) to suppress noise interference. They are thus well adapted for detection of the ultrasonic signals even when they are strongly smeared by the noise or distorted in the medium. A number of tests conducted on simulated and actual ultrasonic signals have demonstrated that ETFDA provides a solid performance.

Keywords: Time-frequency domain average, ultrasonic, peak detection, smoothed pseudo-Wigner-Ville distribution, continuous wavelet transform, Hilbert-Huang transform.

I. INTRODUCTION

Recently, applications of ultrasound have grown significantly in the fields of measurement such as ultrasonic flowmeters, distance or thickness measurement, ultrasonic nondestructive evaluation and ultrasound medical diagnostics, which is due to their robust, intrinsically safe and satisfying accuracy. Most of these applications are based on the estimation of the time of arrival (TOA) and/or time of flight (TOF) of the ultrasonic wave. However, ultrasonic signals generated in the above applications often suffer from some problems such as pollution of noise and other interfering signals, amplitude attenuation and shape distortion of ultrasonic echo.

Various signal processing techniques have been developed in the corresponding literatures. Correlation method [1], matching pursuit [2], Kalman filter [3], model-based estimation method [4], in-phase quadrature (IQ) demodulation [5], continuous wavelet transform (CWT) [6] and empirical mode decomposition (EMD) [7] etc. have been used in the ultrasonic-based applications. The major shortcoming of the cross-correlation method is the unavailability of the reference signal [8]. Noise is another factor which may severely affect the aforementioned techniques. Most of the ultrasonic signals generated by various acoustic transducers in the ultrasonic-based applications are nonstationary. Time-frequency analysis is well adapted to deal with those nonstationary signals. In this paper three novel synchronous averaging of time-frequency distribution have been proposed, which extend the averaging of short-time Fourier transform method presented in [9, 10]. These extended time-frequency domain average (ETFDA) methods which utilize the attractive time-frequency localization characteristics of smoothed pseudo-Wigner-Ville distribution, continuous wavelet transform and Hilbert-Huang transform is well adapted to detect the ultrasonic peaks. The ETFDA is insensitive to noise contained in the signals and can also effectively eliminate the signal disturbance. A number of tests conducted on simulated and actual signals have, in fact, demonstrated that the method provides satisfactory performance.

The rest of this paper is organized as follows. Three time-frequency analysis methods and the ETFDA are introduced in section II. In section III, simulated and actual signals have been used to demonstrate the validation of the proposed ETFDA techniques. Some concluding remarks are summarized in section IV.

II. THE EXTENDED TIME-FREQUENCY DOMAIN AVERAGE

Time-frequency analysis (TFA), which analyses signals in terms of joint time and frequency coordinates, has proven useful in a wide variety of fields. The main goal of the TFA of a signal is to determine the energy concentration (EC) along the frequency axis at each time instance [11]. EC provides time-frequency localization for signals being analyzed.

Smoothed pseudo-Wigner-Ville distribution, continuous wavelet transform and Hilbert-Huang transform which represent three categories of TFA with different energy concentration, are adopted in this work.

A. Smoothed pseudo-Wigner-Ville distribution

As it is well known, Wigner distribution is bilinear and time-frequency shift covariant method which can be observed from Eq. (1) [12]:

$$\begin{array}{ccc} s(t) & \rightarrow & s(t - t_0)e^{j2\pi f_0 t} \\ \downarrow & & \downarrow \\ \Xi_s(t, f) & \rightarrow & \Xi_s(t - t_0, f - f_0) \end{array} \quad (1)$$

Wigner distribution can be interpreted as a short-time Fourier transform with the window matched to the signal [11]:

$$W_s(t, f) \triangleq \int_{-\infty}^{+\infty} s\left(t + \frac{\tau}{2}\right) s^*\left(t - \frac{\tau}{2}\right) e^{-j2\pi f \tau} d\tau \quad (2)$$

Although Wigner distribution has many desirable properties such as high time-frequency resolution, it also has the major limitation for multicomponent signals in terms of copious interference terms. Smoothed pseudo-Wigner-Ville distribution (SPWV) tackles the limitations of Wigner distribution at the expense of reduced resolution. It can be expressed as follows:

$$W_{SPWV}^{n \times n}(t, f) \triangleq \int_{-\infty}^{+\infty} g(u - t) \int_{-\infty}^{+\infty} h(\tau) s\left(u + \frac{\tau}{2}\right) s^*\left(u - \frac{\tau}{2}\right) e^{-j2\pi f \tau} d\tau du \quad (3)$$

where n is the length of the signal, and the symbol \triangleq denotes “by definition”. The time windowing h acts as a smoothing in the frequency domain, while time direction smoothing is implemented by convolving a low-pass function g . The independence of the two window functions enables them to be applied individually, or in combination, so that the desired degree of interference suppression can be achieved. In this work, a Kaiser window of length 31 was employed to weight the received signals in time and frequency domain. The actual ultrasonic signal illustrated in Fig. 1(a) exhibits some strong clutter components due to the installation effect and wall roughness, the pressure flaps in the pipes and acoustic noise produced by the regulator etc. The result using SPWV for a real received signal is illustrated in Fig. 1(b). There we can find not only the visible EC in the SPWV of the signal localized at the 500 kHz frequency but also the false EC.

B. Continuous wavelet transform

Continuous wavelet transform (CWT) is the second category of time-frequency analysis. It has the advantage of being a linear expansion of the signal onto a set of analyzing functions [12]:

$$\begin{aligned}
 s(t) &\rightarrow \frac{1}{\sqrt{a}} s\left(\frac{t-t_0}{a}\right) \\
 \downarrow &\qquad\qquad\qquad \downarrow \\
 \Omega_s(t, f) &\rightarrow \Omega_s\left(\frac{t-t_0}{a}, af\right)
 \end{aligned}
 \tag{4}$$

Those analyzing functions used in the CWT are a family of zero-mean functions obtained by translating and dilating a mother wavelet function. CWT is the simplest time-scale analysis and can be defined as:

$$W_{CWT}^{n \times n}(a, t) \triangleq \frac{1}{\sqrt{a}} \int_{-\infty}^{\infty} s(\tau) \psi^* \left(\frac{t-\tau}{a} \right) d\tau
 \tag{5}$$

where * denotes the complex conjugate and ψ is the mother wavelet. The coefficients $W_{CWT}^{n \times n}(a, t)$ provide a measure of the similitude between the dilated/translated parent wavelet and the signal at time t and scale a .

Many mother wavelet or basis functions can be used in the CWT. The 1-D Gabor wavelets is used in this research, which are constructed with modulating the Gaussian window to a certain frequency:

$$\psi(t) = \frac{1}{\sqrt{2\pi\sigma_t^2}} e^{-\frac{t^2}{2\sigma_t^2}} e^{i2\pi f_0 t}
 \tag{6}$$

Here, σ_t controls the width of the region over which most of the energy is concentrated, f_0 is the center frequency of the filter. In this work, Gaussian function with $\sigma_t = 0.55$ and $f_0 = 0.5$ is employed. Fig. 1(c) provides the result for a real signal by scalogram and the peak is localized at scale 50 (about 500 kHz frequency). Meanwhile, the false ECs are also detected by the CWT. These false ECs may influence the estimated transit time.

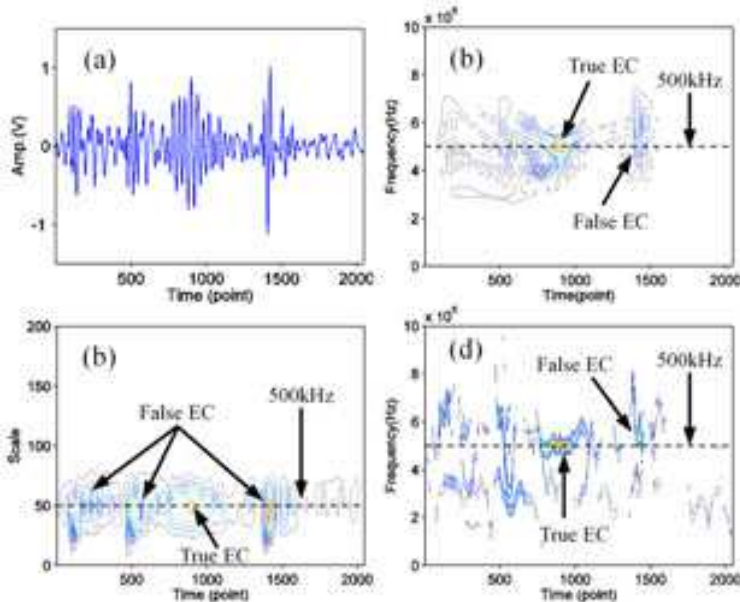


Fig. 1. A real ultrasonic signal and its time – frequency representations: (a) Time domain waveform; (b) SPWVS; (c) Scalogram; (d) HHS

C. Hilbert-Huang transform

The Hilbert-Huang transform (HHT), proposed by Huang et al, is based on two signal processing methods: empirical mode decomposition (EMD) and the Hilbert spectral analysis [13]:

$$\begin{array}{ccc}
 s(t) & \xrightarrow{EMD} & \sum c_i(t) + R(t) \\
 \downarrow & & \downarrow_{HSA} \\
 \Theta_s(t, f) & \rightarrow & \Theta_s(a_i(t), f_i(t))
 \end{array} \tag{7}$$

Firstly, EMD decomposes the signal into several intrinsic mode functions (IMFs). Having obtained the intrinsic mode function (IMF) components, one will have no difficulty in applying the Hilbert transform to each of these IMFs components according to the Eq. (8):

$$H(s(t)) = \frac{1}{\pi} \int_{-\infty}^{\infty} s(\tau) \frac{1}{t - \tau} d\tau \tag{8}$$

Then the original signal can be expressed as the real part in the following form:

$$s(t) = \Re \left(\sum_{j=1}^n a_j(t) e^{i2\pi \int f_j(t) dt} \right) \tag{9}$$

where $a_j(t)$ and $f_j(t)$ are amplitude and frequency of the j th IMF, and $\Re(\cdot)$ denotes the real part. Both amplitude and frequency of each component are functions of time. This phase is called Hilbert spectral analysis. The energy-time-frequency representation of the signal depicted as a color level image is called Hilbert-Huang spectrum (HHS) [13], based on the 2D array $W_{HHT}^{n \times n}$, which combines amplitude $a_j(t)$ and instantaneous frequency $f_j(t)$ together by:

$$W_{HHT}^{n \times n}(f, t) \triangleq (f_i(t), a_j(t))_{i=1, \dots, n, j=1, \dots, n} \tag{10}$$

Thus HHT provides a flexible representation of a dynamic signal by revealing its time-dependent amplitude and characteristic frequency components at various time instances. HHT has been successfully applied to identify the arrival time of overlapping ultrasonic echoes in time-of-flight diffraction flaw detection [7]. Fig. 1(d) presents the Hilbert Huang spectrum of the same signal in Fig. 1(a). It can be found from the Fig. 1(b), (c) and (d) both the true and false ECs have the same frequency (500 kHz) but different duration time.

D. The extended time-frequency domain average

Time domain average (TDA) is a strong signal processing technique based on the synchronization time-domain signal average:

$$\begin{array}{ccc}
 s_i(t), i = 1, \dots, N & \xrightarrow{\frac{1}{N} \sum_i s_i(t)} & TDA(t) \\
 \downarrow_{TFA} & & \\
 T_{s_i}(t, f), i = 1, \dots, N & \xrightarrow{\frac{1}{N} \sum_i T_i(t, f)} & ETFDA(t, f)
 \end{array} \tag{11}$$

It is well known that TDA technique can decrease the influence of noise and improve the signal-to-noise ratio. As mentioned previously, SPWV, scalogram and HHS could produce misleading ECs as they successfully detect the true EC. We combine the TFA with TDA techniques, and propose the extended time-frequency domain average (ETFDA) technique. The three aforementioned time-frequency transforms are applied to calculate the 2D time-frequency

information matrices $W_{T,i}^{n \times n}$. Meanwhile, the average of time-frequency information matrix $\overline{W}_T^{n \times n}$ can be used to suppress the effects caused by those false peaks or the inherent noise. This process is mathematically defined as:

$$\overline{W}_T^{n \times n} = \frac{1}{N} \sum_{i=1}^N W_{T,i}^{n \times n} \quad (12)$$

where N is the size of signal sets, $W_{T,i}^{n \times n}$ is the results for the i th calculated signal and T denotes the adopted transform in Eq. (3), (5) or (10). For example, $W_{SPWV}^{n \times n}$ represents the ETFDA using smoothed pseudo-Wigner-Ville distribution. Employing the ETFDA, the noncoherent component and nonsynchronous components in the successive records of the waveform are averaged out. Furthermore, if the time-frequency information matrix $W_{T,i}^{n \times n}$ is computed respectively by using SPWV, scalogram and HHS, the corresponding ETFDA methodologies are called AVSPWV, AVSG and AVHHS in this paper. Scheme of the proposed three ETFDA techniques is shown in Fig. 2.

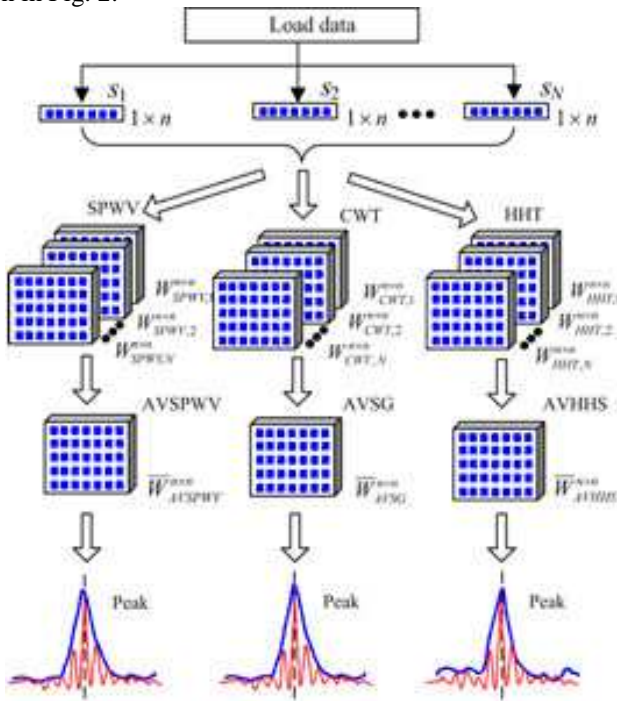


Fig. 2. Scheme of the extended TFDA

III. METHOD VALIDATION

A. Numerical simulation

To test the performance of such proposed ETFDA techniques, a Gaussian echo model in [8] ultrasonic signal is used. This model can be written as:

$$s(\mathcal{G}; t) = \beta e^{-\alpha(t-\zeta)^2} \cos(2\pi f_c(t - \zeta) + \theta) \quad (13)$$

where $\mathcal{G} = [\alpha \ \zeta \ f_c \ \theta \ \beta]$ and parameters α - bandwidth factor, ζ - arrival time, f_c - center frequency, θ - phase, β - amplitude. A simulated ultrasonic signal

containing three Gaussian echo model can be depicted as:

$$y(t) = \sum_{i=1}^3 s(\mathcal{G}_i; t) + \varepsilon(t) \quad (14)$$

where:

$$\begin{aligned} \mathcal{G}_1 &= [0.50 \quad 251 \quad 0.796 \quad 0 \quad 1], \\ \mathcal{G}_2 &= [0.50 \quad 751 \quad 0.796 \quad 0 \quad 40], \\ \mathcal{G}_3 &= [0.50 \quad 1376 \quad 0.796 \quad 0 \quad 0.20] \end{aligned}$$

and $\varepsilon(t)$ is the Gaussian white noise. The simulated noise-free ultrasonic signal is depicted in Fig. 3. There three ultrasonic waves located at 251 ms, 751 ms and 1376 ms can be identified. Gauss white noise is added to the original simulated signals and signal-to-noise is 20 dB in this paper. Fig. 4(a1) presents the time domain representation of all the simulated 20 noisy ultrasonic signals. We can observe that the second and third Gaussian waves are almost buried in the background noise. One of the simulated noisy signals is illustrated in Fig. 4(a2). Figs. 4(b1) & (b2), Figs. 4(c1) & (c2), Figs. 4(d1) & (d2) provide the results of ETFDA as well as their slices on the peaks by using the AVSPWV, AVSG and AVHHS, respectively. It can be observed from the three slice figures that the proposed ETFDA techniques have all detected the ultrasonic waveform. Moreover, the time corresponding to those peaks in Fig. 4(b2) and Fig. 4(c2) are 251, 751 ms, and the time in Fig. 4(d2) is 1377 ms. Thus, these ETFDA techniques are powerful and can effectively detect the ultrasonic signals even under heavy noise.

In-phase quadrature (IQ) demodulation, also known as quadrature demodulation etc, is a conventional technique used in detecting ultrasonic wave [5]. In this paper, low-pass filter with a very narrow bandwidth and high stopband attenuation is chose in the IQ demodulation, which may be produced by Hanning windowed sinc filter. As can be seen from Fig. 5(a) and (b) (one of the demodulated signal), IQ demodulation can also remove the Gauss white noise and detect the peaks of the ultrasonic wave.

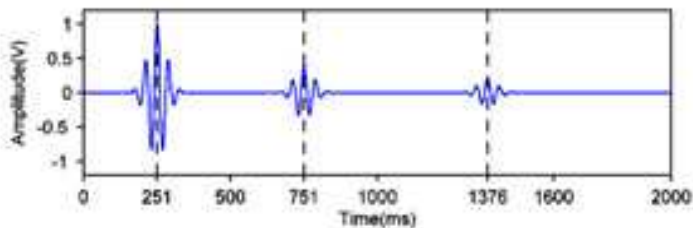


Fig. 3. Simulated noise – free ultrasonic signal

B. Experimental results

Many ultrasonic-based applications such as ultrasonic flow measurements are based on the estimation of the time of arrival (TOA) and/or time of flight (TOF) of the ultrasonic pulse-echo. Detecting ultrasonic peaks is usually the key in this time differential ultrasonic flowmeters. Ultrasonic flowmeter is one of the fastest growing technologies within the general field of instruments for process monitoring, control, and measurement [14].

It should be noted that the primary interest of this paper lies in detecting the ultrasonic wave in general ultrasonic-based applications rather than focusing on a particular application area such as measuring the flow velocity. We use this experiment to verify and validate the proposed ETFDA techniques. However, if further applications of the ETFDA are conducted, flow rate may be calculated even for the distorted ultrasonic signals, which may still be a challenge for the clamp-on ultrasonic flowmeter using the existing methodologies so far. The

measurement configuration used in this work is depicted in Fig. 6. One pair of transducers was face-to-face clamped to the pipeline ($\text{Ø}6$ inch). The 500 kHz working frequency of ultrasonic transducers proves to be the most suitable to avoid noise effects [15]. This frequency is above the noise level detected in gas pipelines. Moreover, the signal loss due to attenuation of ultrasound in gas is still negligible [15]. Gas flow velocity was varied by adjusting drive motor frequency (MF) and increased with the MF. The fluctuation of temperature of medium may affect the measured signals. Thus, there is a cooling system available in the rig to maintain an approximately constant temperature (about 70-80° F).

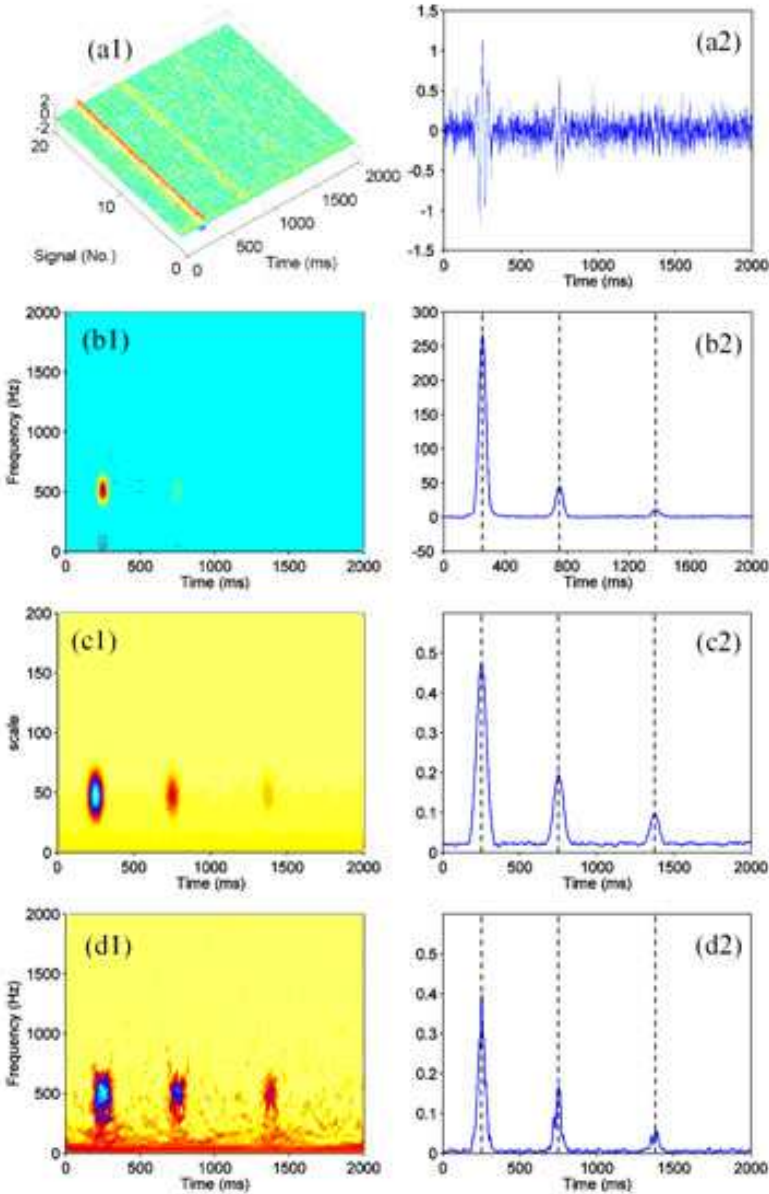


Fig. 4. (a1) 3D show of 20 simulated noisy ultrasonic signals; (a2) one temporal signal of (a1); (b1) AVSPWV; (b2) peaks detection of (b1); (c1) AVSG; (c2) peaks detection of (c1); (d1) AVHHS; (d2) peaks detection of (d1)

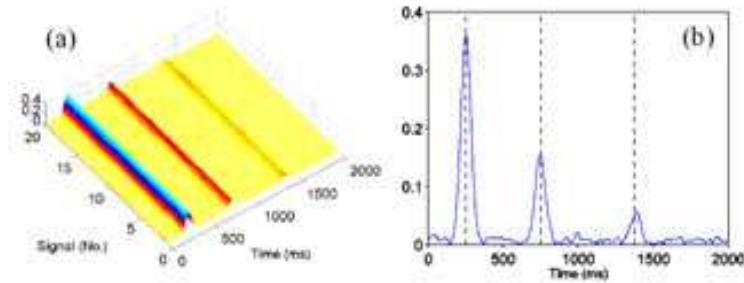


Fig. 5. (a) 3D show of IQ demodulated ultrasonic signals; (b) one IQ demodulated signal of (a)

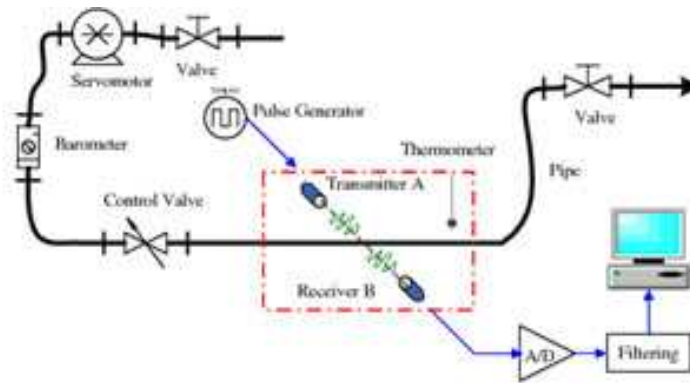


Fig. 6. Experimental set – up for ultrasonic gas flowmeter

When a transmitting sensor is excited by a single-pulse trigger, the transmitted signal begins to oscillate at the working frequency (500 kHz) and its amplitude increases rapidly first and then begins to decrease gradually. The received signal after conversion and low-pass filtering with 2.5 MHz cut-off frequency was recorded by a PC. However, ultrasonic flow measurements for gas are, compared to those for liquid, characterized by large signal fluctuations, which may render in poor tracking. The received signals experience low signal-to-noise ratio and degradation of their shapes, due to the low pressure (0 psig), high gas flow velocities (121.6 ft/s) etc. Nevertheless, as will be revealed in this subsection, ultrasonic embedded in those distorted signals can still be identified by using the proposed ETFDA.

Sampling frequency and length is set to 20 MHz and 2048 in this experiment, respectively. For each gas pressure $P=0, 5, 15$ and 50 psig and $MF=60$ Hz, 80 data sets of downstream (A→B) and upstream (B→A) shown in Fig. 6 are recorded and prepared for the following analysis. Fig. 7 presents 3D plot of all the measured 80 signals in each case. It can be observed that the received signals are poor with the decrease of the gas pressure. And, in particular, the received upstream (B→A) ultrasonic signals provided in Fig. 7(a2) are almost smeared in the disturbed clutters as $P=0$ psig. Fig. 8 indicates the results of the acquired ultrasonic signals using the IQ demodulation. It demonstrates that clutters and other disturbed components still exist in the demodulated signals in the case of low gas pressure and high flow rate. Because clutters in the ultrasonic wave have the same modulated frequency with the objects of interest, IQ demodulation can not remove the effects of the clutter.

The results of TDA of all the acquired signals are illustrated in Fig. 9. The IQ demodulation results of TDA signals are illustrated in Fig. 10. Similarly, we can observe that both TDA and

IQ demodulation techniques cannot effectively detect the ultrasonic when the gas pressure is 0 psig (shown in Figs. 9(a) and 10(a)). The reason is that signal degradation caused by high flow velocity (121.6 ft/s) and low pressure (0 psig) can not be revealed by TDA, then IQ demodulation cannot effectively identify the ultrasonic wave. In fact, it is still a challenge to detect ultrasonic for clamp-on gas flowmeter as pressure reduces to 0 psig. Thus we mainly focus on the case of the low pressure ($P=0$ psig and 5 psig) in the following analysis.

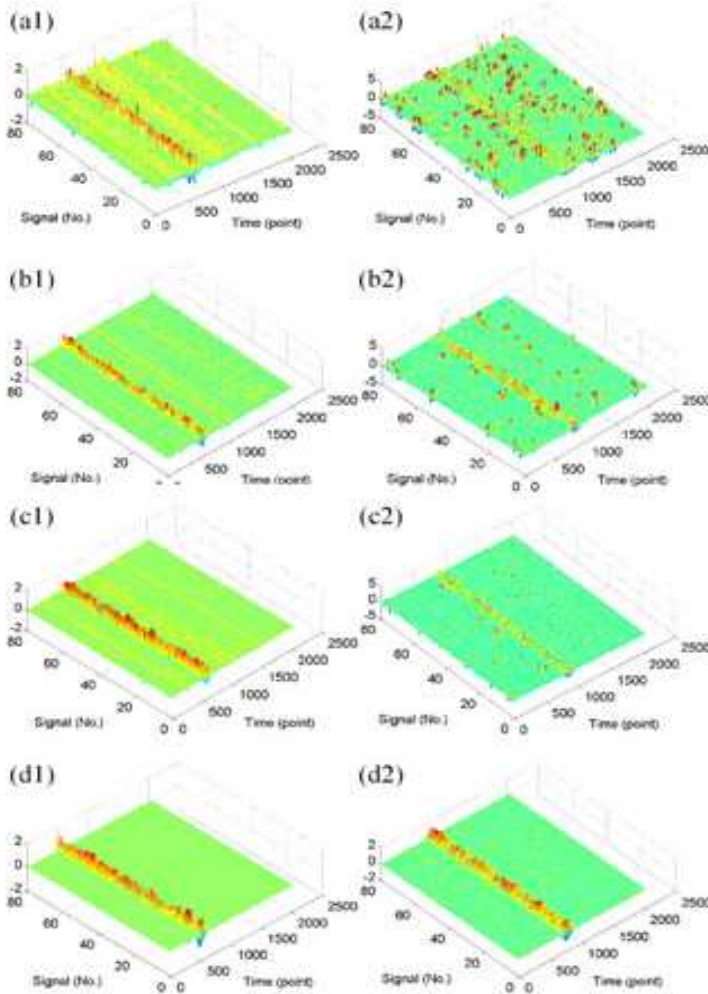


Fig. 7. 3D show of 80 real received ultrasonic signals with MF = 60 Hz and P = 0, 5, 15 and 50 psig (from the top down): (a1) – (d1) Downstream (A→B); (a2) – (d2) Upstream (B→A)

Using the ETFDA techniques proposed in section II, the contour plots of AVSPWV, AVSG and AVHHS for the received upstream and downstream signals in the case of MF=60 Hz and P=0 psig are depicted individually in Figs. 11(a), (c) and (e). It can be observed that two ECs are visible over 500 kHz frequency (or scale 50 in Fig. 11(b)) region of interest and false ECs are greatly restrained by the proposed techniques. Figs 11(b), (d) and (f) illustrate the profiles of the Figs. 11(a), (c) and (e) on the peaks corresponding to 500 kHz frequency, respectively. Based on the ETFDA, peaks of the upstream and downstream signals located at 611 and 868 in Fig. 11(b), 611 and 869 in Fig. 11(c), 609 and 863 in Fig. 11(d). Thus the proposed ETFDA

techniques successfully detect the ultrasonic signals even at the existence of strong signal disturbance.

For gas pressure $P=5$ psig and $MF=60$ Hz the results of application of ETFDA are illustrated in Figs. 12(a), (c) and (e). Again, we can observe the major ECs in the time-frequency contour plots are also concentrated in the region of 500 kHz (or scale 50 in Fig. 12(b)) frequency. In addition, peaks of the upstream and downstream waveform are located at 587 and 861 in Fig. 12(b), 588 and 863 in Fig. 12(c), 586 and 860 in Fig. 12(d). Meanwhile, we can clearly observe that the results within the first or the second data sets are almost identical, but the time difference between two peaks for the first data set ($P=0$ psig) is not same with the second one ($P=5$ psig). This error may be caused by the fluctuation of the temperature. In these experiments, temperature is only controlled in the range of 70-80° F. Moreover, it is difficult to keep the temperature absolutely stable, because high speed may produce more heat and the longer test may also make the temperature different.

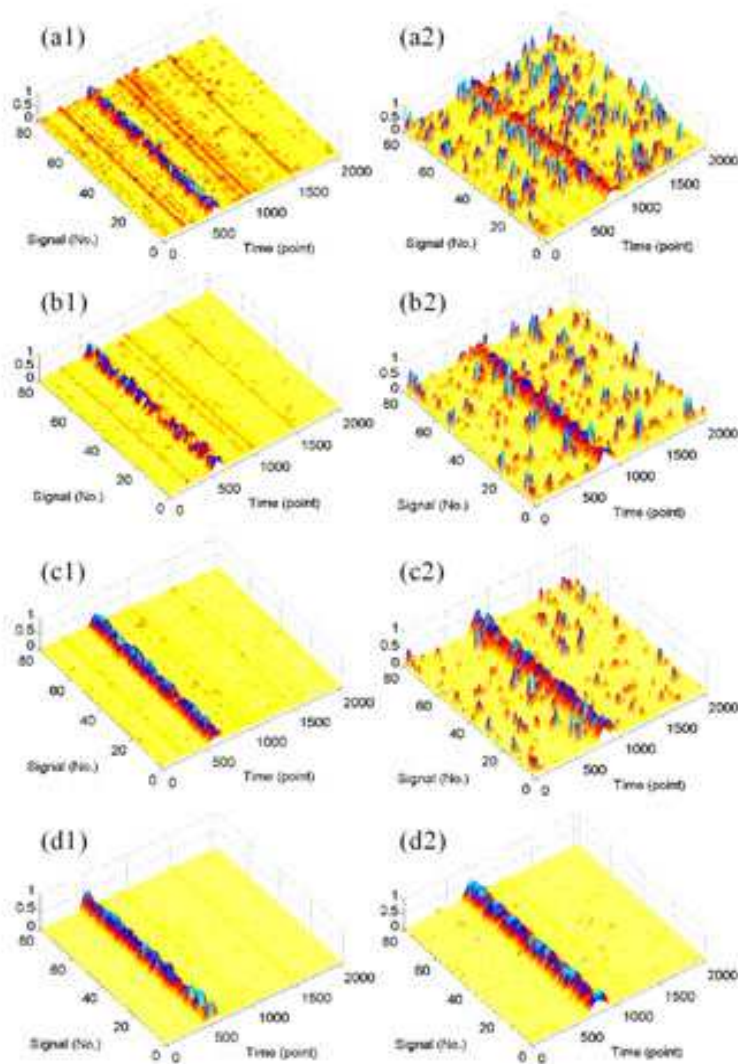


Fig. 8. Results of the ultrasonic signals in Fig. 6 using IQ demodulation (from the top down): (a1) – (d1) Downstream (A → B); (a2) – (d2) Upstream (B → A)

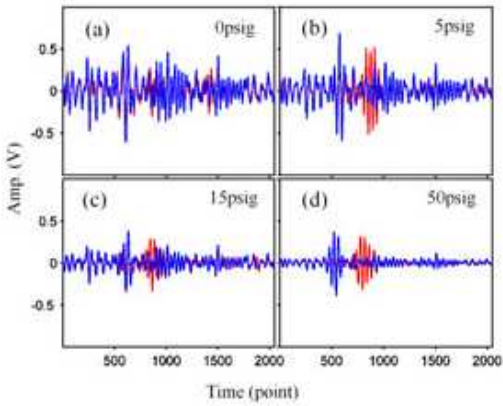


Fig. 9. TDA for the real received ultrasonic signals in Fig. 6: blue solid, downstream (A → B); red solid, upstream (B → A)

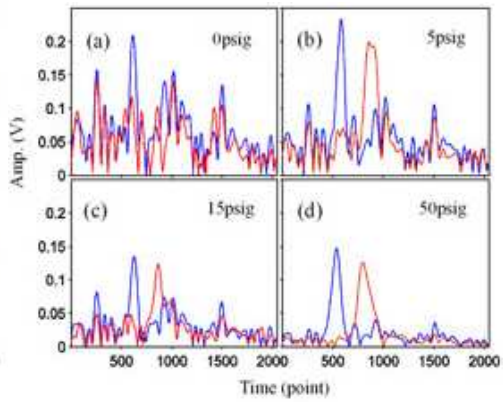


Fig. 10. Results of the TDA signals in Fig. 7 using IQ demodulation, blue solid: downstream (A → B); red solid: upstream (B → A)

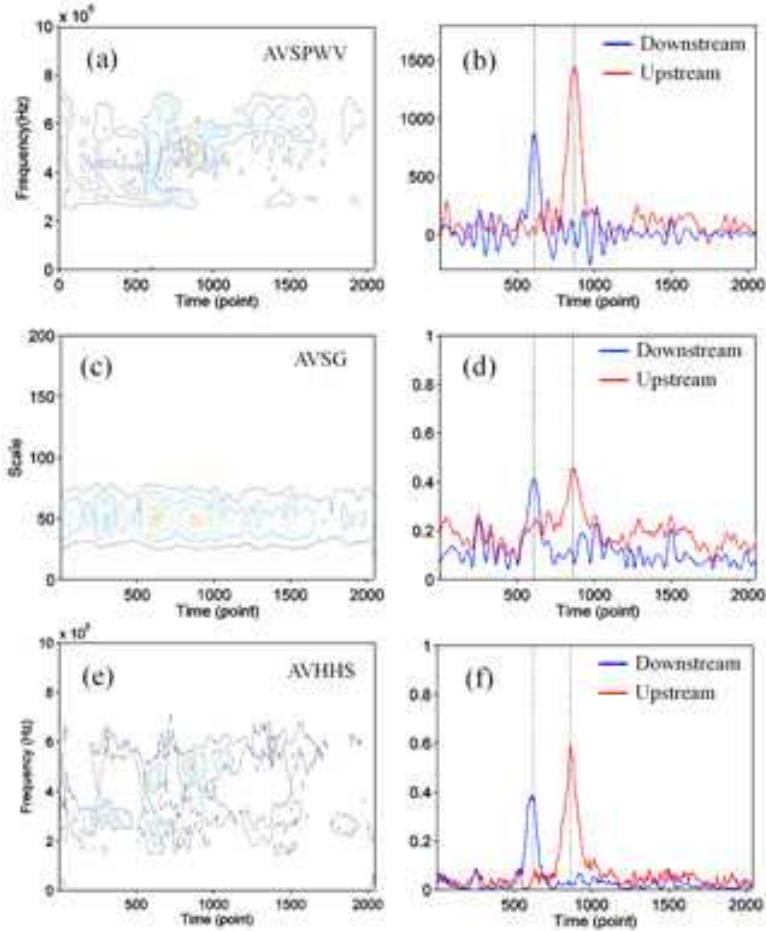


Fig. 11. Contour show of signals in Figs. 6 (a1) & (a2) by using Extended TFDA and their time – frequency profiles on the peaks: (a) AVSPWV, (b) profile of (a); (c) AVSG, (d) profile of (c); (e) AVHHS, (f) profile of (e)

IV. CONCLUSION AND DISCUSSION

Since ultrasound has gained extensive applications in the fields of measurements, an immediate problem is to solve ultrasonic wave detection when the received signals are contaminated with noise or other interfering signals. Based on the smoothed pseudo-Wigner-Ville distribution, continuous wavelet transform and Hilbert-Huang transform, three ETFDA methods have been presented for the ultrasonic detection. The ETFDA techniques utilize effective time-frequency localization characteristics of the three time-frequency transforms and ability of the TDA to suppress noise interference. The performance of these ETFDA have been assessed through a number of both simulated ultrasonic tests and actual ultrasonic signals acquired from a clamp-on ultrasonic gas flowmeter with pressure as low as 0 psig. The ETFDA is verified to be insensitive to clutter contained in the signals, and it can also effectively and exactly eliminate strong signal disturbance.

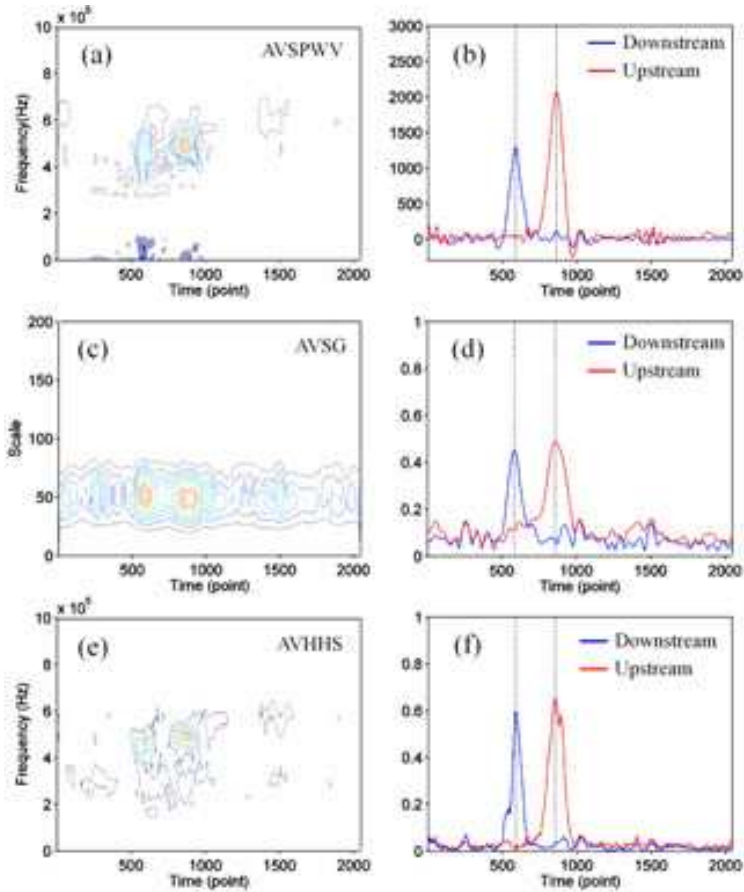


Fig. 12. Contour show of signals in Figs. 6 (b1) & (b2) by using Extended TFDA and time – frequency profiles on the peaks: (a) AVSPWV, (b) profile of (a); (c) AVSG, (d) profile of (c); (e) AVHHS, (f) profile of (e)

ETFDA can be also utilized to other ultrasonic applications such as ultrasonic medical diagnostics. Ultrasound provides a less harmful but certainly effective method for *in vivo* assessment. Its usefulness as a tool to aid medical diagnosis can be improved by removing the various acoustic noises and artifacts that commonly arise from reverberation and multi-path

reflection as it travels across or around highly reflective objects or interfaces. Therefore, these ETFDA techniques may have a significant potential for ultrasonic-based applications.

ACKNOWLEDGMENTS

This research is supported financially by the key project of National Natural Science Foundation of China (No. 50335030) and National Natural Science Foundation of China (No. 50805028).

References

- [1] **Y. Y. Lin and V. Hans**, "Self-monitoring ultrasonic gas flow meter based on vortex and correlation method", *IEEE Trans. Instrum. Meas.*, vol. 56, pp. 2420-2424, 2007.
- [2] **W. Liang, P.-W. Que, H.-M. Lei, and L. Chen**. "Matching pursuit for decomposition and approximation of ultrasonic pulse-echo wavelet and its application in ultrasonic nondestructive evaluation", *Rev. Sci. Instrum.*, vol. 79, pp. 1-7, 2008.
- [3] **L. Angrisani, A. Baccigalupi, and R. S. Lo Moriello**. "A measurement method based on Kalman filtering for ultrasonic time-of-flight estimation", *IEEE Trans. Instrum. Meas.*, vol. 55, pp. 442-448, 2006.
- [4] **R. Demirli and J. Saniie**. "Model-based estimation of ultrasonic echoes part II: Nondestructive evaluation applications", *IEEE Trans. Ultrason. Ferroelectr. Freq. Control*, vol. 48, pp. 803-811, 2001.
- [5] **L. Adgrisani and R. S. L. Moriello**. "Estimating ultrasonic time-of-flight through quadrature demodulation", *IEEE Trans. Instrum. Meas.*, vol. 55, pp. 54-62, 2006.
- [6] **L. Bechou, D. Dallet, Y. Danto, P. Daponte, Y. Ousten, and S. Rapuano**. "An improved method for automatic detection and location of defects in electronic components using scanning ultrasonic microscopy", *IEEE Trans. Instrum. Meas.*, vol. 52, pp. 135-142, 2003.
- [7] **T. L. Chen, P. W. Que, Q. Zhang, and Q. K. Liu**. "Ultrasonic signal identification by empirical mode decomposition and Hilbert transform", *Rev. Sci. Instrum.*, vol. 76, 2005.
- [8] **R. Demirli and J. Saniie**. "Model-based estimation of ultrasonic echoes part I: Analysis and algorithms", *IEEE Trans. Ultrason. Ferroelectr. Freq. Control*, vol. 48, pp. 787-802, 2001.
- [9] **E. B. Halim, S. L. Shah, M. J. Zuo, and M. Choudhury**. "Fault detection of gearbox from vibration signals using time-frequency domain averaging", presented at Proc. 2006 American Control Conference, Minneapolis, Minnesota, 2006.
- [10] **L. M. Zhu, H. Ding, and X. Y. Zhu**. "Synchronous averaging of time-frequency distribution with application to machine condition monitoring", *ASME Journal of Vibration and Acoustics*, pp. 441-7, 2007.
- [11] **L. Cohen**, *Time-frequency analysis*. New York: Prentice Hall, 1995.
- [12] **P. Goncalves and R. G. Baraniuk**. "Pseudo affine Wigner distributions: Definition and kernel formulation", *IEEE Trans. Signal Process.*, vol. 46, pp. 1505-1516, 1998.
- [13] **N. E. Huang, Z. Shen, and S. R. Long**. "A new view of nonlinear water waves: the Hilbert spectrum", *Annu. Rev. Fluid. Mech.*, vol. 31, pp. 417-457, 1999.
- [14] **D. V. Mahadeva, R. C. Baker, and J. Woodhouse**. "Further studies of the accuracy of clamp-on transit-time ultrasonic flowmeters for liquids", *IEEE Trans. Instrum. Meas.*, pp. 1602-1609, 2009.
- [15] **P. Brassier, B. Hosten, and F. Vulovic**. "High-frequency transducers and correlation method to enhance ultrasonic gas flow metering", *Flow Meas. Instrum.*, vol. 12, pp. 201-211, 2001.